Received: 6 July 2023 | Revised: 27 October 2023 | Accepted: 22 November 2023

DOI: 10.1002/ar.25361

RESEARCH ARTICLE

The Anatomical Record WILEY

Ecological correlates of three-dimensional muscle architecture within the dietarily diverse Strepsirrhini

Edwin Dickinson[1,2] | **Madison Manzo**[1] | **Cassidy E. Davis**[1] | **Shruti Kolli**[1,3] | **Alysa Schwenk**[1,4] | **Ashley Carter**[1] | **Cindy Liu**[1] | **Nimi Vasipalli**[1] | **Aleksandra Ratkiewicz**[2] | **Ashley R. Deutsch**[1] | **Michael C. Granatosky**[2,5] | **Adam Hartstone-Rose**[1]

[1]Department of Biological Sciences, North Carolina State University, Raleigh, North Carolina, USA

[2]Department of Anatomy, College of Osteopathic Medicine, New York Institute of Technology, Old Westbury, New York, USA

[3]Department of Biological Sciences, University of Denver, Denver, Colorado, USA

[4]College of Public Health, Thomacharles Jefferson University, Philadelphia, Pennsylvania, USA

[5]Center for Biomedical Innovation, College of Osteopathic Medicine, New York Institute of Technology, Old Westbury, New York, USA

Correspondence
Adam Hartstone-Rose, Department of Biological Sciences, North Carolina State University, Raleigh, NC, USA.
Email: adamhrose@ncsu.edu

Funding information
the National Sciences Foundation, Grant/Award Number: IOS-5-57125; New York Institute of Technology

Abstract

Analysis of muscle architecture, traditionally conducted via gross dissection, has been used to evaluate adaptive relationships between anatomical form and behavioral function. However, gross dissection cannot preserve three-dimensional relationships between myological structures for analysis. To analyze such data, we employ diffusible, iodine-based contrast-enhanced computed tomography (DiceCT) to explore the relationships between feeding ecology and masticatory muscle microanatomy in eight dietarily diverse strepsirrhines: allowing, for the first time, preservation of three-dimensional fascicle orientation and tortuosity across a functional comparative sample. We find that fascicle properties derived from these digital analyses generally agree with those measured from gross-dissected conspecifics. Physiological cross-sectional area was greatest in species with mechanically challenging diets. Frugivorous taxa and the wood-gouging species all exhibit long jaw adductor fascicles, while more folivorous species show the shortest relative jaw adductor fascicle lengths. Fascicle orientation in the parasagittal plane also seems to have a clear dietary association: most folivorous taxa have masseter and temporalis muscle vectors that intersect acutely while these vectors intersect obliquely in more frugivorous species. Finally, we observed notably greater magnitudes of fascicle tortuosity, as well as greater interspecific variation in tortuosity, within the jaw adductor musculature than in the jaw abductors. While the use of a single specimen per species precludes analysis of intraspecific variation, our data highlight the diversity of microanatomical variation that exists within the strepsirrhine feeding system and suggest that muscle architectural configurations are evolutionarily labile in response to dietary ecology—an observation to be explored across larger samples in the future.

KEYWORDS
anatomy, DiceCT, feeding, lemurs, PCSA

1 | INTRODUCTION

Muscular anatomy, on both the macro- and micro-scale, is intrinsically related to muscle function (Gans & Bock, 1965; Schumacher, 1961; Turnbull, 1970). As such, quantifying skeletal muscle within a comparative context represents a critical means of bridging the divide between form and function (Anapol & Barry, 1996; Gans, 1982; Hartstone-Rose et al., 2018; Kikuchi, 2010; Lieber & Fridén, 2000; Marchi et al., 2018; Payne et al., 2006). In recent years, numerous studies have highlighted the potential of diffusible, iodine-based contrast-enhanced computed tomography (DiceCT) in facilitating the relatively non-destructive quantification of muscle microarchitecture while preserving spatial data on internal muscle organization (Dickinson et al., 2019; Dickinson, Kolli, et al., 2020; Dickinson, Stark, & Kupczik, 2018; Gignac et al., 2016). However, owing to limited sample sizes, such studies have lacked a direct framework within which to interpret novel streams of data such as three-dimensional orientation or fascicular tortuosity—that is, curvature, or the difference between a fascicle's chord length and arc length. Here, we present a comparative study of eight dietarily diverse strepsirrhines—the largest comparative sample of taxa to ever be studied via DiceCT analysis of fascicle architecture—to directly explore relationships between feeding ecology and masticatory muscle microanatomy in three-dimensional space. We further compare digitally reconstructed fascicle properties to previously published reports derived from traditional gross dissection of conspecifics from each taxon. Finally, we outline a theoretical framework within which to interpret data on fascicle orientation and tortuosity from a functional perspective.

1.1 | Muscle architecture and function

Both gross-scale and microarchitectural components of skeletal muscle contribute to its contractile properties. Skeletal muscle is composed of bundles of muscle fibers, or fascicles, which are themselves individually composed of serially arranged sarcomeres: the contractile units of muscle (Gans, 1982; Gans & Bock, 1965; Lieber, 1986; Powell et al., 1984). As sarcomeres contract simultaneously, and sarcomere lengths are conservative across mammals, longer fascicles exhibit a greater excursion potential and contractile speed (Bang et al., 2006; Gokhin et al., 2009; Lieber & Fridén, 2000). Within the masticatory musculature, therefore, increasing fascicle length facilitates both a greater maximum gape and a faster jaw-closing velocity. However, increasing fascicle lengths reduces the total number of fascicles that can be accommodated within a given volume of muscle and, by extension, the magnitude of contractile force a muscle may generate (Gans & Bock, 1965; Schumacher, 1961). This force-generating potential can be estimated anatomically by a muscle's physiological cross-sectional area (PCSA): a multivariable function of muscle mass, density, and fiber length (Anapol et al., 2008; Anapol & Barry, 1996; Brand et al., 1986). Thus, there exists a functional trade-off within muscle architecture between contractile force and excursion/velocity potential that is governed by the length of fascicles.

Muscle architectural properties within the masticatory apparatus have been explored in a dietary context across myriad taxa, including reptiles (Herrel & O'Reilly, 2006; Huyghe et al., 2009; Pfaller et al., 2011), birds (Carril et al., 2015; Gussekloo & Bout, 2005; Sakamoto et al., 2019), mammalian carnivorans (Hartstone-Rose et al., 2012; Hartstone-Rose et al., 2019; Hartstone-Rose et al., 2022; Penrose et al., 2020), and primates (Antón, 1999, 2000; Deutsch et al., 2020; Dickinson, Fitton, & Kupczik, 2018; Eng et al., 2009; Hartstone-Rose et al., 2018; Perry et al., 2011; Perry et al., 2014; Taylor et al., 2009; Taylor & Vinyard, 2009; Taylor & Vinyard, 2013; Terhune et al., 2015). Within strepsirrhines specifically, a positive relationship is reported between fascicle lengths in the jaw adductor muscles and food item size, such that taxa consuming larger foods show correspondingly longer fascicles to support a wider gape (Perry et al., 2011). Physiological cross-sectional area is also reported to scale with positive allometry relative to body mass in folivores, but isometrically in frugivores and insectivores, suggesting an increase in relative masticatory force potential among tough-food specialists (Perry et al., 2011). In both old and new-world monkeys, fascicle lengths and food item size were similarly reported to co-vary, though these taxa do not exhibit the same correlation between jaw adductor PCSA and dietary mechanical resistance (Hartstone-Rose et al., 2018).

1.2 | Digital reconstructions of myology

While the majority of muscle architectural data in primates—and indeed, muscle architectural data in general—has been

collected using traditional gross dissection techniques, recent studies have sought to quantify masticatory anatomy using DiceCT (Gignac et al., 2016; Jeffery et al., 2011; Metscher, 2009). This technique uses slow permeation of iodine to bind with the glycogen of muscle fascicles but not to the collagenous perimysium, thus allowing for discrimination between individual fascicles in a muscle (Dickinson, Stark, & Kupczik, 2018; Gignac et al., 2016; Li et al., 2015). As a relatively non-destructive and reversible technique, DiceCT further facilitates analysis of specimens that would otherwise be unsuitable for dissection (Early et al., 2020; Lanzetti & Ekdale, 2021; Morhardt & Witmer, 2016). As such, numerous studies over the past decade have utilized DiceCT to describe muscle attachment areas, define layers within muscle groups, and measure whole-muscle volumes (e.g., Baverstock et al., 2013; Cox & Faulkes, 2014; Cox & Jeffery, 2011; Dickinson, Atkinson, et al., 2020; Holliday et al., 2013; Sahd et al., 2022; Santana, 2018; To et al., 2021).

At finer resolutions, several attempts have been made to quantify the architectural properties of masticatory muscles from DiceCT datasets: employing either manual (Dickinson et al., 2019; Dickinson, Kolli, et al., 2020) or algorithmic (Dickinson, Stark, & Kupczik, 2018; Holliday et al., 2022; Katzke et al., 2022; Sullivan et al., 2019) approaches to visualizing fascicles. In so doing, such studies have sought to quantify the concordance between data generated via gross dissection vs. digital dissection (Dickinson et al., 2019; Dickinson, Stark, & Kupczik, 2018). While these comparative studies have served to validate these digital techniques, later studies (e.g., Dickinson, Kolli, et al., 2020) have also highlighted the potential value of quantifying three-dimensional fascicle orientation within a functional context; by preserving spatial orientation in situ, such datasets make it possible to define the force vectors of individual muscles and the extent of fascicular heterogeneity within and between muscle groups. However, such data are reported in only three primate taxa (*Callithrix jacchus*, *Eulemur mongoz*, and *Daubentonia madagascariensis*; Dickinson et al., 2019; Dickinson, Kolli, et al., 2020) and thus lack a broader comparative framework to link three-dimensional orientation with any ecological parameter, such as diet.

Strepsirrhines represent an ideal framework for exploring such questions. Within a constrained phylogeny and body mass range, strepsirrhines span a considerable breadth of dietary specializations (Table 1): from frugivores (e.g., *Eulemur*; Chen et al., 2015) and folivores (e.g., *Propithecus*; Richard, 1977) to generalist omnivores (e.g., *Lemur*; Kay et al., 1978), tree-gougers (e.g., *Daubentonia*; Erickson, 1994) and obdurate bamboo specialists (e.g., *Hapalemur*; Yamashita et al., 2009). Within this study, we present digital reconstructions of the masticatory musculature across eight strepsirrhine taxa (Table 1) chosen specifically to span a wide spectrum of diets and cranial morphologies. Within this sample, we analyze both traditional (e.g., fascicle lengths and PCSA) and novel (e.g., 3D fascicular orientation and tortuosity) architectural variables in three-dimensional space—the first DiceCT study to do so. We test the following.

1.3 | Aims and predictions

Prediction 1: relative fascicle lengths and PCSA (after adjusting for body size) will vary interspecifically in relation to diet. Comparative gross dissections of masticatory muscles in strepsirrhines have suggested a tight relationship between muscle architecture and diet, with greater relative masticatory force potential among tough-food specialists and relatively longer fascicles among taxa that habitually consume larger foods (Perry et al., 2011). We thus anticipate a similar finding within our own digitally derived dataset, predicting relatively high PCSA values in obdurate diet taxa such as *H. griseus* and *P. coquereli* and relatively high fascicle lengths in the frugivorous *Varecia variegata* and the gouging *D. madagascariensis*.

Prediction 2: Heterogeneity in fascicle orientations will increase in taxa with more mechanically challenging diets. Data on three-dimensional fascicle orientation are yet to be assessed within a substantial comparative and functional framework, yet some inferences may be drawn by considering how diet may impact movements of the jaw. For example, while fruits and insects can likely be crushed using simple jaw adduction, mature foliage and bamboo are quite tough (Yamashita et al., 2009) and likely require significant lateral grinding in the mouth to process. Similarly, *D. madagascariensis* practices tree-gouging, a mechanically demanding activity that necessitates complex three-dimensional movements of the mandible (Toler & Wall, 2013). Thus, we anticipate that taxa with more complex and demanding masticatory loading regimes (i.e., folivores and gougers) will exhibit more heterogenous fascicle orientations between muscles than frugivores or insectivores.

Prediction 3: Tortuosity will be greatest in species that frequently consume larger foods. As with fascicle orientation, since this is the first study to explore three-dimensional muscle architecture across a substantial comparative sample, expectations regarding tortuosity are largely grounded in theory. In functional terms, tortuosity within a fascicle represents compression or "slack": as the jaw opens, this slack in the mandibular adductors is taken up and the fascicle decompresses to its true length. As the jaw continues to open, the adductor fascicle then stretches beyond its resting length. These changes in fascicle length

TABLE 1 Sample. Body masses from Mittermeier et al., 2013 (sex-specific mass where available). (For more specimen information, including original designations, contact authors).

Species	Spec. #	Body mass (g)	Diet	Dietary notes
Otolemur garnettii	AHR 111021	800	Omnivory	Diet is split approximately equally between insects (∼50%) and fruits (∼50%). Common insects include grasshoppers, crickets, mantids, centipedes, and various beetles; common fruits include *Ficus*, *Lannea*, *Grewia*, and *Meyna* (Harcourt & Nash, 1986).
Daubentonia madagascariensis	AHR 112002	2500	Gouging (insectivory)	Typically consume wood-boring larvae via "tap-foraging," a technique in which the third digit is tapped against bark to identify cavities, after which the wood is gnawed away using the incisors (Erickson, 1991, 1994; Sterling, 1994). Seeds, nectar, and fungus are also consumed (Sterling, 1994).
Propithecus coquereli	AHR 113016	3300	Folivory (foliage)	Typical consumption includes a high proportion of leaves, including mature foliage (∼50% of diet), supplemented where available by assorted fruits (∼35%), flowers (∼10%), and other miscellanies (Campbell et al., 2004; Sato et al., 2016).
Varecia variegata	AHR 114043	3450	Frugivory	Highly frugivorous (>60% of diet), supplemented by leaves and flowers. Common fruits include *Calophyllum*, *Ficus*, and *Garcinia* (Britt, 2000; Martinez & Razafindratsima, 2014).
Eulemur coronatus	AHR 114035	1300	Frugivory	Highly frugivorous (∼90% of diet; ripe fruit = 60%, unripe fruit = 30%). Most commonly *Ficus*, *Artocarpus*, *Pachytrophe*, and *Streblus* (Chen et al., 2015).
Eulemur mongoz	AHR 114038	1200	Frugivory/Omnivory	Predominantly frugivorous (∼65%) supplemented by leaves (15%), nectar (10%) and flowers (5%). Mature fruits dominate in the wet season, while mature and immature fruits are exploited equally in the dry season (Curtis, 2004).
Hapalemur griseus	AHR 114021	900	Folivory (bamboo)	Folivorous, specializing in bamboo (∼80% of diet; Grassi, 2006). Other frequently consumed foods include fruits such as *Ficus*, *Gaertnera*, and various genera of guava (Myrtaceae).
Lemur catta	AHR 114042	2250	Omnivory	Variable/omnivorous (∼40% of diet fruits, both ripe and unripe; ∼40% leaves, including both young and mature foliage (Simmen et al., 2003; Simmen et al., 2006).

affect contractile properties following each fascicle's length-tension curve. While high tortuosity likely reduces contractile potential at jaw occlusion (by compressing fibers within the fascicle to sub-optimal lengths on the L-T curve), it may function to shift the window of optimal force production to wider gapes. Thus, we predict that greater tortuosity may represent an adaption toward biting at wide gapes and should subsequently be greatest among wood-gougers and frugivores, diets that have been previously tied to increased gape potential (Dickinson, Kolli, et al., 2020; Perry et al., 2011).

2 | MATERIALS AND METHODS

Our sample consists of eight adult strepsirrhines (Table 1; Figure 1), obtained from the Duke Lemur Center (Durham, NC), the Lemur Conservation Foundation (Myakka City, FL), and the Cincinnati Zoo (Cincinnati, OH). All specimens arrived frozen with intact crania and were thawed and then fixed upon receipt in a bath of 10% buffered formalin solution with the jaws in a standardized posture of jaw occlusion. Skin was not removed prior to fixation. All specimens presented in good muscular

TABLE 2 Myological parameters measured within this study. Muscle abbreviations as follows: superficial masseter (SM), deep masseter (DM), zygomaticomandibularis (ZM), superficial temporalis (ST), deep temporalis (DT), zygomatic temporalis (ZT), medial pterygoid (MP); lateral pterygoid (LP), anterior digastric (AD), posterior digastric (PD). Literature data was collected from Perry et al., 2011 for seven species and from Perry et al., 2014 for *Daubentonia*.

Species	Muscle	Mass (g)	PCSA (cm^2)	Lit. FL (mm)	Chord FL (mm)	Arc FL (mm)	Tortuosity (%)	Parasagittal angle (°)	Paracoronal angle (°)
Otolemur garnettii	SM	1.34	1.51	8.5	7.80 ± 1.69	8.39 ± 1.65	107.95 ± 4.61	28.22 ± 16.25	43.83 ± 13.45
	DM	0.45	0.69	8.8	6.54 ± 0.81	6.88 ± 0.80	105.30 ± 3.19	47.64 ± 10.93	31.50 ± 8.71
	ZM	0.67	1.34	7.0	5.13 ± 0.82	5.38 ± 0.81	104.83 ± 2.60	139.84 ± 12.27	62.56 ± 9.20
	ST	1.5	1.94	8.8	7.74 ± 1.43	8.29 ± 1.64	106.86 ± 3.05	137.61 ± 11.31	332.31 ± 9.76
	DT	1.82	2.39	7.4	7.47 ± 1.77	8.18 ± 1.88	109.91 ± 5.34	151.29 ± 17.14	315.34 ± 16.75
	ZT	0.36	0.64	9.0	5.72 ± 1.16	6.05 ± 1.13	106.24 ± 3.86	175.47 ± 18.66	54.29 ± 16.72
	MP	0.69	1.21	5.7	5.68 ± 0.72	6.02 ± 0.89	105.68 ± 4.11	41.24 ± 15.42	323.42 ± 13.56
	LP	0.15	0.37	–	3.93 ± 1.35	4.11 ± 1.47	104.45 ± 3.17	346.81 ± 23.99	275.86 ± 36.62
	AD	0.08	0.25	–	3.38 ± 1.34	3.52 ± 1.43	103.92 ± 1.14	23.50 ± 5.30	334.65 ± 5.14
	PD	0.21	0.41	–	5.23 ± 1.10	5.49 ± 1.26	104.62 ± 2.99	154.41 ± 9.17	31.97 ± 11.31
Daubentonia madagascariensis	SM	3.16	2.39	8.42	11.76 ± 2.74	12.59 ± 2.84	107.31 ± 3.32	34.53 ± 13.43	39.25 ± 18.56
	DM	1.33	1.34	8.27	10.37 ± 2.23	10.91 ± 2.37	105.08 ± 2.99	56.43 ± 5.49	27.85 ± 6.45
	ZM	0.40	0.41	9.26	9.73 ± 2.65	10.31 ± 2.79	106.23 ± 4.53	107.90 ± 10.65	35.21 ± 5.59
	ST	6.97	4.42	12.96	15.21 ± 5.66	16.88 ± 6.59	111.05 ± 8.54	138.40 ± 28.20	339.13 ± 7.13
	DT	6.02	4.94	14.74	11.92 ± 5.73	13.24 ± 6.36	112.13 ± 8.28	142.49 ± 17.17	343.38 ± 27.07
	ZT	1.27	0.93	9.58	13.81 ± 3.24	15.07 ± 3.43	109.15 ± 5.24	109.16 ± 34.22	45.88 ± 10.47
	MP	2.06	1.88	5.9	10.75 ± 2.20	11.55 ± 2.32	107.53 ± 3.32	75.18 ± 4.97	339.3 ± 3.39
	LP	0.86	0.77	–	11.24 ± 3.97	11.70 ± 4.04	104.34 ± 3.33	6.12 ± 17.71	280.83 ± 19.21
Propithecus coquereli	SM	1.87	1.41	10.4	12.00 ± 1.61	12.59 ± 1.54	105.20 ± 3.19	54.29 ± 7.57	22.73 ± 5.35
	DM	0.78	1.05	7.6	7.44 ± 2.19	7.83 ± 2.43	104.90 ± 2.03	58.67 ± 10.94	40.89 ± 12.38
	ZM	1.03	1.54	6.1	6.67 ± 1.05	7.06 ± 1.12	105.79 ± 1.60	124.48 ± 18.06	57.51 ± 4.37
	ST	1.28	1.61	6.5	7.90 ± 1.70	8.54 ± 1.90	108.22 ± 3.81	161.33 ± 29.70	321.07 ± 22.66
	DT	1.71	2.35	7.7	7.14 ± 2.40	7.69 ± 2.62	107.68 ± 4.15	154.61 ± 19.69	310.34 ± 17.81
	ZT	0.45	0.56	7.6	8.21 ± 1.65	8.59 ± 1.73	104.58 ± 0.83	146.14 ± 14.81	63.82 ± 7.71
	MP	1.02	1.97	5.7	5.28 ± 1.20	5.47 ± 1.24	103.76 ± 2.05	69.11 ± 7.82	344.81 ± 7.39
	LP	0.48	0.80	–	6.11 ± 1.31	6.34 ± 1.42	103.54 ± 2.21	17.88 ± 28.04	274.35 ± 31.90
	AD	0.23	0.64	–	3.73 ± 1.34	3.84 ± 1.39	102.73 ± 1.56	29.60 ± 10.02	31.09 ± 9.53
	PD	0.23	0.38	–	6.08 ± 1.46	6.23 ± 1.39	103.09 ± 2.95	148.32 ± 9.95	19.48 ± 8.57

(Continues)

TABLE 2 (Continued)

Species	Muscle	Mass (g)	PCSA (cm^2)	Lit. FL (mm)	Chord FL (mm)	Arc FL (mm)	Tortuosity (%)	Parasagittal angle (°)	Paracoronal angle (°)
Varecia variegata	SM	2.15	1.85	12.4	10.12 ± 2.12	10.98 ± 2.03	109.03 ± 4.38	17.90 ± 12.31	53.48 ± 27.42
	DM	0.23	0.27	9.7	8.14 ± 1.47	8.87 ± 1.84	108.67 ± 5.40	42.93 ± 8.04	20.81 ± 4.75
	ZM	0.58	0.73	9.4	7.60 ± 1.89	8.38 ± 1.97	110.45 ± 4.56	81.21 ± 4.50	44.17 ± 5.61
	ST	1.98	1.58	14.9	11.69 ± 2.32	13.25 ± 2.19	114.10 ± 5.48	157.56 ± 31.91	339.07 ± 10.58
	DT	3.86	3.12	13.9	11.86 ± 1.51	13.07 ± 0.94	110.99 ± 7.49	157.20 ± 22.82	273.68 ± 7.25
	ZT	0.58	0.62	11.1	9.14 ± 2.10	9.90 ± 2.14	108.61 ± 3.21	84.54 ± 13.96	275.36 ± 56.75
	MP	1.00	1.07	8.4	9.39 ± 2.43	9.87 ± 2.46	105.35 ± 3.52	29.38 ± 11.73	331.44 ± 24.65
	LP	0.18	0.29	–	6.54 ± 0.94	6.80 ± 1.04	103.80 ± 2.11	11.10 ± 7.87	249.69 ± 13.64
	AD	0.25	0.29	–	8.99 ± 2.31	9.27 ± 2.26	103.39 ± 2.93	9.60 ± 7.44	346.61 ± 5.82
	PD	0.27	0.37	–	7.54 ± 0.55	7.67 ± 0.59	101.81 ± 0.78	141.76 ± 7.50	16.3 ± 6.66
Eulemur coronatus	SM	1.33	1.43	8.2	8.62 ± 2.24	8.91 ± 2.22	103.84 ± 3.94	22.63 ± 12.87	56.01 ± 19.17
	DM	0.35	0.53	7.8	6.41 ± 1.72	6.87 ± 1.88	106.99 ± 4.33	40.55 ± 10.45	32.26 ± 5.88
	ZM	0.19	0.35	6.2	5.46 ± 1.19	5.95 ± 1.37	108.88 ± 4.03	130.23 ± 12.52	49.57 ± 8.32
	ST	0.94	0.83	11.2	11.69 ± 3.17	12.60 ± 3.40	108.70 ± 5.74	156.4 ± 14.47	306.64 ± 27.66
	DT	2.01	1.99	9.6	9.86 ± 1.61	10.87 ± 1.48	109.49 ± 6.25	144.55 ± 25.58	314.21 ± 26.57
	ZT	0.18	0.24	7.2	7.16 ± 1.80	7.86 ± 1.96	109.62 ± 5.41	177.71 ± 18.07	57.97 ± 13.73
	MP	0.61	0.98	5.8	6.07 ± 2.68	6.59 ± 2.86	109.38 ± 4.22	38.05 ± 9.31	325.20 ± 13.43
	LP	0.17	0.25	–	6.80 ± 1.42	7.08 ± 1.45	104.26 ± 2.66	6.43 ± 9.16	265.11 ± 16.93
	AD	0.13	0.16	–	8.34 ± 3.70	8.76 ± 4.01	104.60 ± 4.02	11.98 ± 3.49	342.79 ± 10.27
	PD	0.14	0.14	–	9.84 ± 4.84	10.27 ± 5.01	104.85 ± 3.19	138.42 ± 6.29	13.99 ± 7.82
Eulemur mongoz	SM	1	1.29	10.3	6.58 ± 2.33	7.33 ± 2.84	110.08 ± 5.54	34.96 ± 7.01	34.31 ± 6.63
	DM	0.36	0.6	6.5	5.64 ± 2.34	6.25 ± 2.35	112.53 ± 7.50	69.58 ± 9.51	32.98 ± 3.28
	ZM	0.22	0.27	4.5	8.29 ± 1.76	8.77 ± 1.70	106.21 ± 4.55	107.63 ± 5.98	49.41 ± 8.44
	ST	1.18	1.24	10	9.05 ± 3.93	9.91 ± 4.17	111.02 ± 6.55	155.39 ± 25.60	304.65 ± 18.83
	DT	1.65	1.81	8.8	8.76 ± 3.07	9.81 ± 3.38	112.39 ± 4.85	152.4 ± 28.03	344.71 ± 3.47
	ZT	0.36	0.42	3.6	8.35 ± 3.96	8.97 ± 4.27	107.36 ± 3.78	148.71 ± 22.28	33.15 ± 4.11
	MP	0.75	1.22	5.7	6.26 ± 2.83	6.74 ± 3.09	107.74 ± 4.59	59.95 ± 10.35	328.54 ± 2.69
	LP	0.13	0.23	–	5.67 ± 2.56	5.76 ± 2.58	101.59 ± 2.13	359.65 ± 14.19	288.23 ± 5.31
Hapalemur griseus	SM	1.13	1.63	9.4	6.33 ± 1.08	6.57 ± 1.10	103.86 ± 2.64	43.45 ± 7.75	35.69 ± 12.34
	DM	0.28	0.45	7.7	6.20 ± 1.79	6.50 ± 1.86	105.00 ± 4.30	66.89 ± 11.49	23.43 ± 6.95

TABLE 2 (Continued)

Species	Muscle	Mass (g)	PCSA (cm^2)	Lit. FL (mm)	Chord FL (mm)	Arc FL (mm)	Tortuosity (%)	Parasagittal angle (°)	Paracoronal angle (°)
	ZM	0.52	0.96	4.8	5.62 ± 1.56	5.80 ± 1.56	103.58 ± 3.03	106.43 ± 7.70	23.43 ± 6.95
	ST	0.37	0.49	9.7	7.48 ± 1.61	8.11 ± 1.73	108.48 ± 3.64	137.35 ± 21.16	317.35 ± 13.21
	DT	1.26	2.14	8.7	5.86 ± 1.20	6.31 ± 1.06	108.50 ± 7.06	151.11 ± 30.21	309.44 ± 14.71
	ZT	0.32	0.42	7	7.68 ± 1.46	8.08 ± 1.25	105.97 ± 4.56	131.02 ± 19.87	46.33 ± 6.69
	MP	0.72	1.18	4.9	6.18 ± 1.76	6.40 ± 1.73	104.00 ± 3.16	42.28 ± 17.12	298.90 ± 10.92
	LP	0.16	0.44	–	3.72 ± 0.74	3.82 ± 0.77	102.65 ± 0.86	36.26 ± 13.11	318.42 ± 14.24
	AD	0.1	0.24	–	4.09 ± 0.79	4.20 ± 0.86	102.82 ± 1.43	18.99 ± 7.81	340.2 ± 7.93
	PD	0.11	0.27	–	4.38 ± 0.57	4.50 ± 0.64	102.65 ± 3.25	147.91 ± 11.62	20.31 ± 15.35
Lemur catta	SM	2.31	2.43	9.8	8.59 ± 1.43	9.01 ± 1.53	104.91 ± 2.56	32.53 ± 10.79	32.71 ± 13.10
	DM	0.25	0.3	9.9	8.50 ± 1.54	8.82 ± 1.41	104.17 ± 3.81	55.24 ± 7.00	29.79 ± 5.29
	ZM	0.59	0.83	7.5	7.07 ± 1.19	7.43 ± 1.05	105.67 ± 5.22	109.29 ± 11.01	45.82 ± 16.23
	ST	0.97	1.1	11.3	8.61 ± 1.13	9.44 ± 1.41	109.46 ± 4.02	134.31 ± 12.47	315.62 ± 13.42
	DT	2.63	2.62	11.3	10.07 ± 1.65	10.83 ± 1.57	107.92 ± 5.14	139.45 ± 15.59	308.15 ± 4.79
	ZT	0.48	0.65	9.8	7.39 ± 0.68	7.76 ± 0.82	105.03 ± 4.65	159.08 ± 16.90	64.62 ± 11.36
	MP	0.61	0.84	6.6	7.37 ± 1.91	7.67 ± 1.97	104.14 ± 1.71	38.17 ± 12.62	325.37 ± 13.32
	LP	0.13	0.28	–	4.86 ± 0.90	5.01 ± 0.96	102.97 ± 1.84	358.21 ± 18.88	270.51 ± 17.08
	AD	0.14	0.31	–	4.50 ± 0.62	4.69 ± 0.72	103.96 ± 3.38	27.68 ± 4.63	344.85 ± 3.05
	PD	0.17	0.46	–	3.67 ± 0.67	3.80 ± 0.68	103.54 ± 2.96	139.67 ± 13.95	14.99 ± 3.67

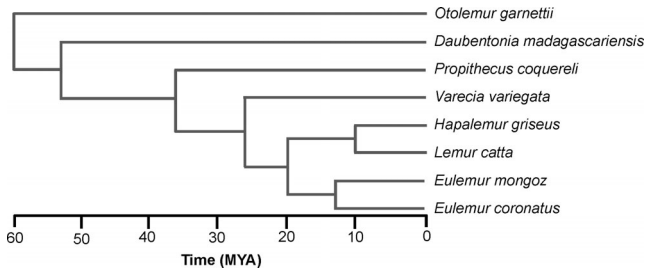

FIGURE 1 Phylogenetic diagram depicting the relationships between samples. For full information on each taxon, see Table 1.

health with no visible atrophy/wastage of muscle tissue. Following fixation (which lasted for 5–10 days, varying based on specimen size, and was assessed by visual and tactile assessment of the tissue), specimens were prescanned to visualize their skeletal anatomy. Two specimens (*D. madagascariensis* and *E. mongoz)* were scanned using a North Star Imaging (NSI) μCT system housed at the University of Texas. The remaining specimens were microCT-scanned using a Nikon XTH-225-ST μCT system housed at Duke University's Shared Materials Instrumentation Facility, or using a Zeiss Xradia 510 Versa 3D Tomography System housed at North Carolina State University's Analytical Instrumentation Facility. Scans of the two aforementioned specimens (*D. madagascariensis* and *E. mongoz*) were previously used in a comparative study (Dickinson, Kolli, et al., 2020) on muscle fascicle architecture, but this previous dataset has been refined to align with the more advanced segmentation methods used here. As such, some minor variation in fascicle lengths is observed between the data presented here and the original study. All other specimens were collected and scanned de novo specifically for use in this study.

After prescanning was complete, each specimen was immersed in a prewash solution of 10% wt/vol sucrose dissolved in distilled water to minimize shrinking during the contrast staining process (Gignac et al., 2016). The specimen remained immersed in this solution for approximately 48 h at room temperature and was then transferred to a low-concentration (1.75–2.5%) Lugol's Iodine (I_2KI) solution, where it remained for several weeks. In order to ensure that the superficial layers of the muscles were not overstained before the deeper portions of the musculature were fully stained (Gignac et al., 2016), a low concentration of Lugol's Iodine (I_2KI) solution was selected. This was also done to further minimize iodine-induced changes in muscle volume (Vickerton et al., 2013). While minor shrinkage may also be associated with formalin fixation (Leonard et al., 2022), recent work has demonstrated that following careful fixation, this effect is minor and does not prevent comparisons between fixed-and-stained and frozen tissues (Dickinson, Kolli, et al., 2020). Test scans were performed on each specimen during the staining process to assess progress. In addition, each specimen was lightly destained in distilled water for a few days prior to scanning to prevent the overstaining of superficial layers and produce an even contrast gradient between deep and superficial tissues. All specimens were rescanned (as described above) following staining (as described above). In order to conduct the digital dissection phase of the process on muscles with as even saturation density as possible throughout the entire depth of the specimen, the two largest specimens (*P. coquereli* and *V. variegata*) required two postscans to be collected: the first postscan was conducted to visualize the superficial muscles, following which the specimens were returned to their staining solution for a further month before a second scan was conducted to further visualize the deeper muscle fascicles.

CT scans (both prescans and postscans) were reconstructed into image stacks in 16-bit using isometric voxel sizes between 0.039 and 0.066 mm. Following Dickinson et al., 2019 and Dickinson, Kolli, et al., 2020, the stained and unstained μCT images were integrated via manual landmark registration (in which the same craniodental features were highlighted in both image stacks) to merge the datasets into a single composite volume for the purposes of visualization. The resultant stained images were then segmented in Amira 6.5 (Visualization Sciences Group, 2018) using a combination of manual and semi-automatic techniques: where fascicular boundaries were easily discernible, the wand tool was utilized to automatically segment fascicles; elsewhere, fascicles and volumes were manually isolated using the brush tool.

Ten muscle subdivisions were "digitally dissected," including both jaw adductors and abductors. The adductor muscles analyzed were as follows: the masseter complex (comprised of the superficial masseter, deep masseter, and zygomaticomandibularis), the temporalis complex (comprised of the superficial temporalis, deep temporalis, zygomatic temporalis); and the medial pterygoid. The abductor muscles included both anterior and posterior bellies of the digastric, as well as the lateral pterygoid; the latter of which aids in abduction via enabling anterior translation (i.e., protrusion) of the mandible (Turnbull, 1970). Whole-muscle volumes were first segmented for each of these muscle portions. Subsequently, individual fascicles from each muscle were segmented, with an average of 10–15 representative fascicles analyzed from throughout each muscle portion (Figures 2–4; Video 1). While algorithmic efforts to resolve muscle fascicles (e.g., see Kupczik et al., 2015; Dickinson Stark, & Kupczik, 2018; Ratkiewicz et al., 2023; Dickinson et al., 2023) typically measure higher numbers of fascicles (>100 per muscle), the automatic nature of this fascicle generation inherently increases the risk of error. Instead, we measure a comparable number of

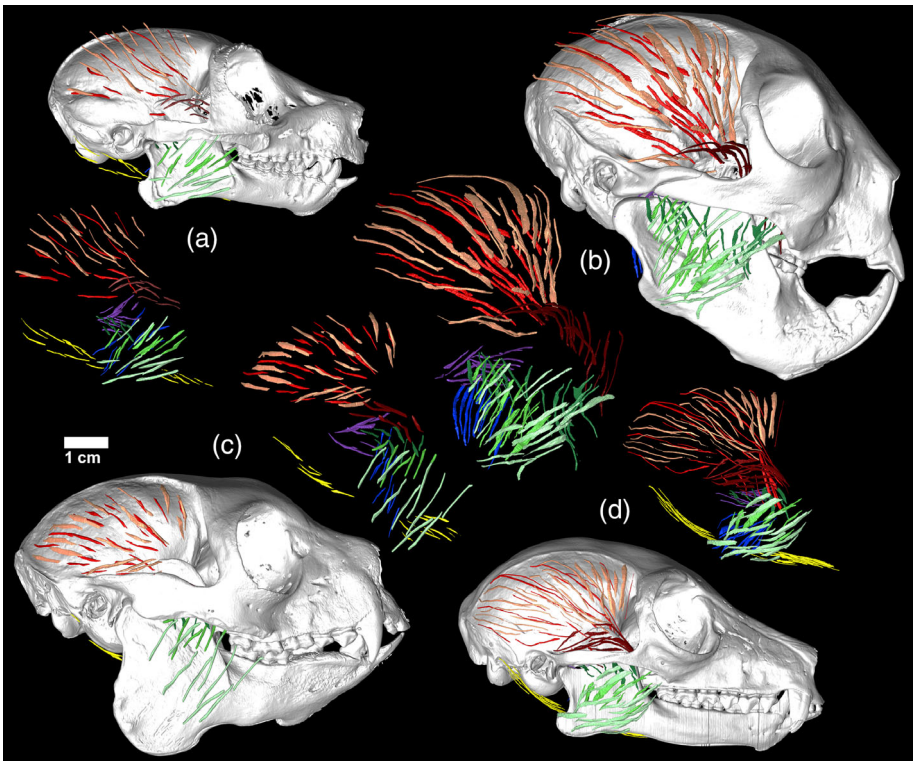

FIGURE 2 Lateral view of muscle fascicles in situ and in isolation of (a) *Otolemur garnettii*, (b) *Daubentonia madagascariensis*, (c) *Propithecus coquereli*, and (d) *Eulemur coronatus*. Fascicle colors are as follows: superficial masseter (light green), deep masseter (green), zygomaticomandibularis (dark green), superficial temporalis (pink), deep temporalis (light red), zygomatic temporalis (dark red), medial pterygoid (blue), lateral pterygoid (purple), anterior and posterior digastric (yellow).

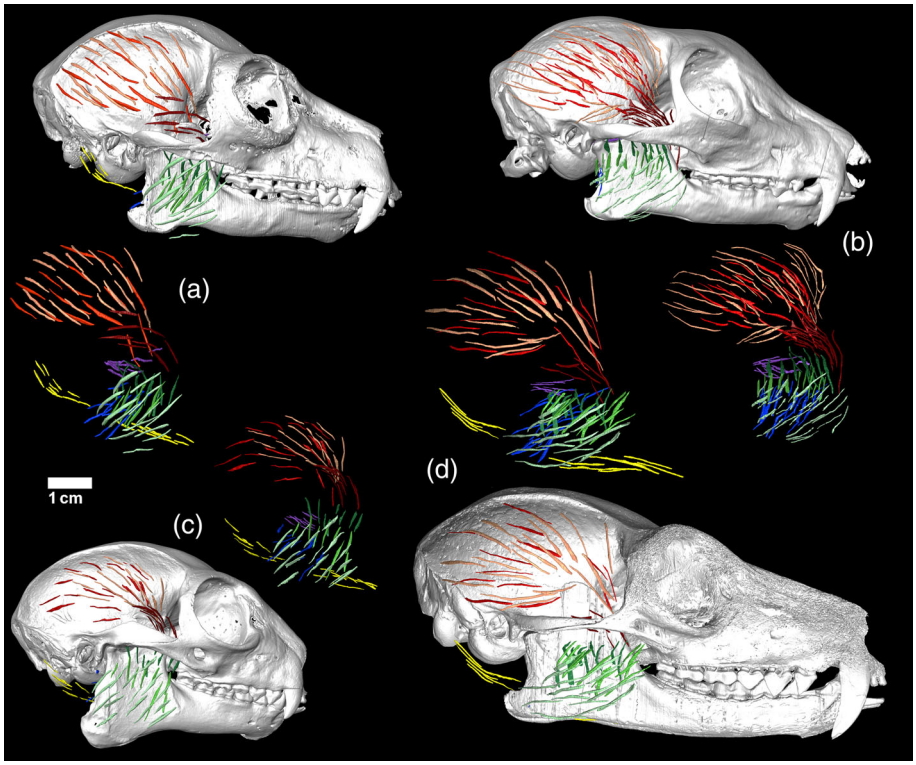

FIGURE 3 Lateral view of muscle fascicles in situ and in isolation of (a) *Lemur catta*, (b) *Eulemur mongoz*, (c) *Hapalemur griseus*, and (d) *Varecia variegata*. Fascicle colors are as follows: superficial masseter (light green), deep masseter (green), zygomaticomandibularis (dark green), superficial temporalis (pink), deep temporalis (light red), zygomatic temporalis (dark red), medial pterygoid (blue), lateral pterygoid (purple), anterior and posterior digastric (yellow).

fascicles to gross dissection, sacrificing quantity for confidence in quality; further, reducing the number of fascicles makes it visually much more straightforward to visually identify individual fascicles and ascertain overarching trends relating to either the orientation or lengths of fascicles. The angle of each fascicle was measured in relation to two planes: the parasagittal plane defined by the Frankfurt horizontal with 0° oriented rostrally and increasing superiorly and the paracoronal plane defined by the cranial midline with 0° oriented vertically and

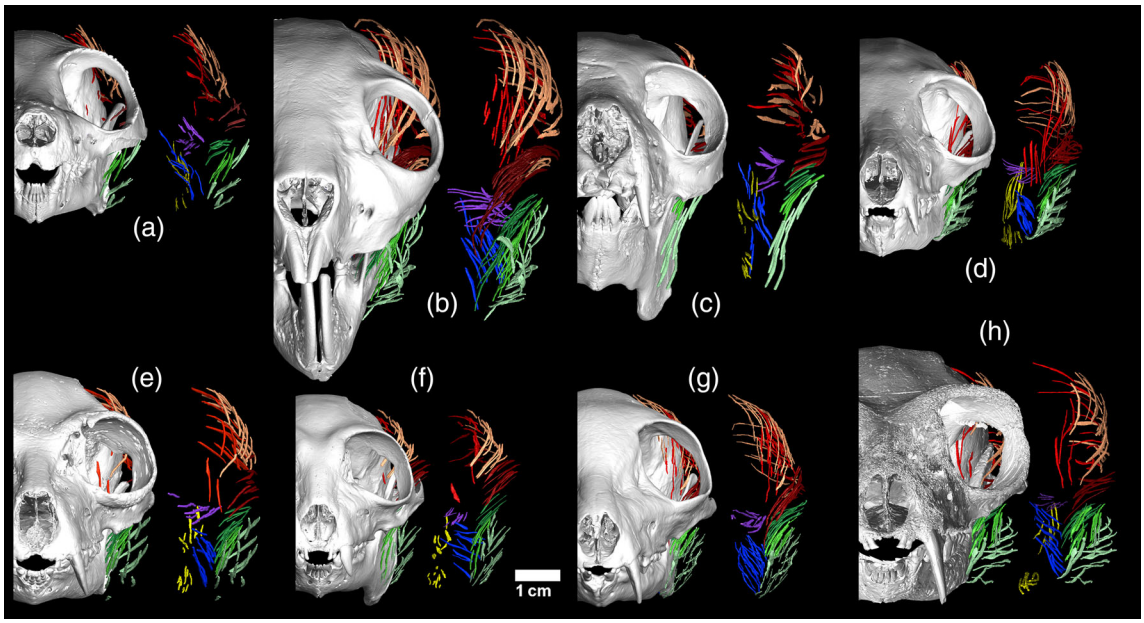

FIGURE 4 Anterior view of muscle fascicles in situ and in isolation of (a) *Otolemur garnettii*, (b) *Daubentonia madagascariensis*, (c) *Propithecus coquereli*, (d) *Eulemur coronatus*, (e) *Lemur catta*, (f) *Eulemur mongoz*, (g) *Hapalemur griseus*, and (h) Varecia variegata). Fascicle colors are as follows: superficial masseter (light green), deep masseter (green), zygomaticomandibularis (dark green), superficial temporalis (pink), deep temporalis (light red), zygomatic temporalis (dark red), medial pterygoid (blue), lateral pterygoid (purple), and anterior and posterior digastric (yellow).

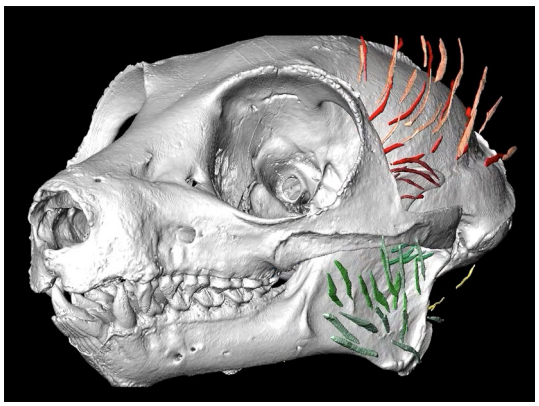

VIDEO 1 Rotational views of fascicles in situ and in isolation of taxa as labeled.
Video content can be viewed at https://onlinelibrary.wiley.com/doi/10.1002/ar.25361

increasing laterally (Figures 5 and 6). For each muscle subdivision, the average angle and its force constant—the product of the muscle's PCSA (derived from the measured digitally dissected volumes and fascicle lengths) times the muscle force constant of 30 N (Weijs & Hillen, 1985)—was plotted on volume rendering of the skulls in these two planes along with combined vectors of the masseter and temporalis respectively (thicker vector lines; Figures 5 and 6). These were calculated with their paracoronal and parasagittal angles established as the weighted averages of the fascicle angles of constituent parts of their complexes and the sum of their forces. Fascicle lengths were measured in two ways using reconstructions of smoothly rendered (constrained smoothing, intensity 3) individual fascicles in Amira: as a chord length from end-to-end, and as a total (arc) length which included the curvature of the fascicles where present. The ratio of these lengths (i.e., tortuosity) was then calculated to define fascicle curvature/compression at occlusion. Finally, to account for variation in size between taxa, sex-specific body masses (where known; otherwise an average was used) for each specimen were derived from the literature (Mittermeier et al., 2013) and used in regression analyses to compare relative (arc) fascicle lengths and PCSA between species. All statistical analyses were performed using JMP 15.0 (SAS, Cary, NC).

3 | RESULTS

3.1 | Comparisons with earlier reports

Comparisons between digitally reconstructed and measured fascicle lengths (Figure 7, red) and fascicles measured from gross-dissected conspecifics by Perry et al., 2011 and Perry et al., 2014 (Figure 7, blue) show generally good agreement (note that while Perry et al.

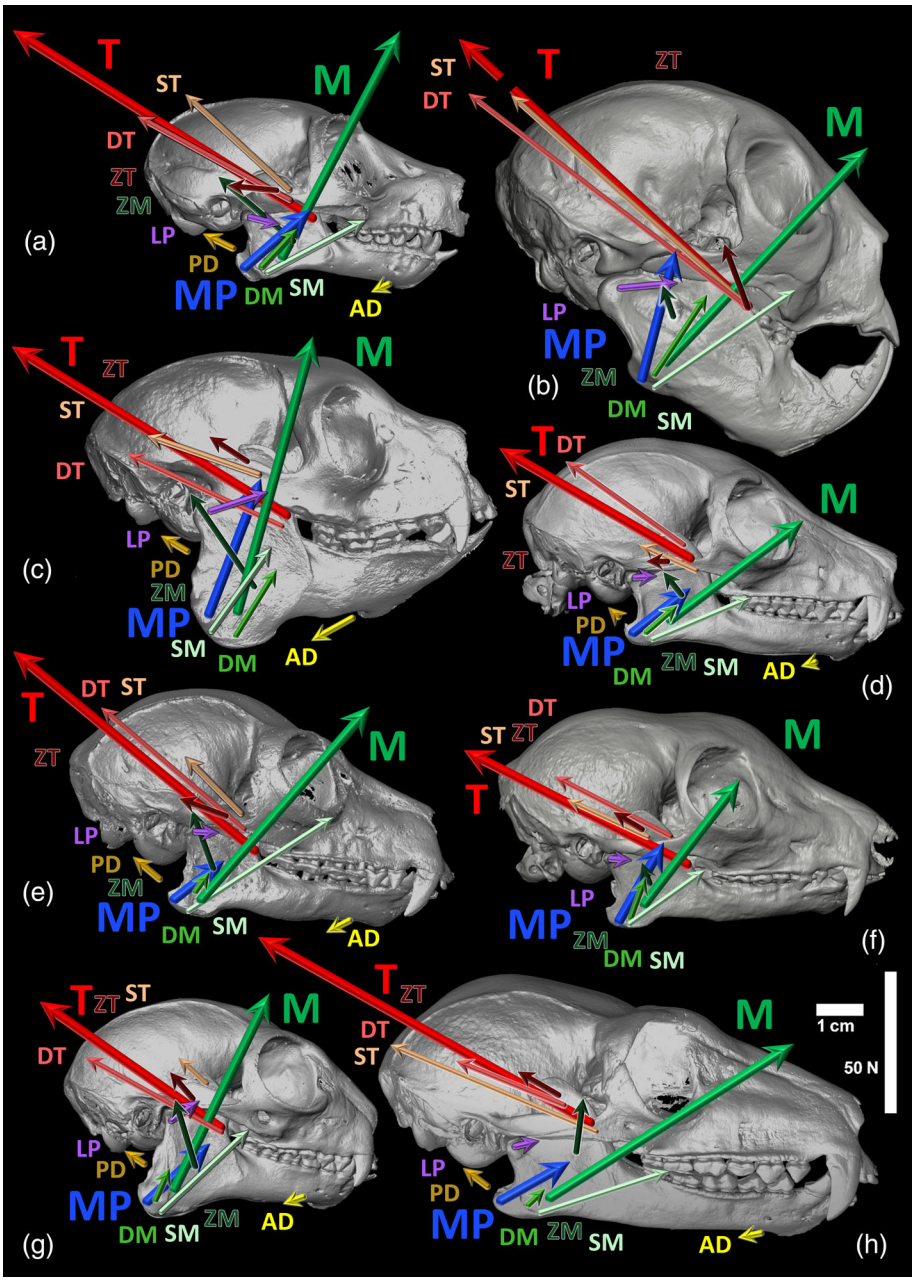

FIGURE 5 Lateral view of muscle vectors, depicting both parasagittal orientation and magnitude (see scale bars). Specimen identification and muscle vector coloration follow Figure 3; in addition, vectors of the masseter complex (M) and temporalis complex (T) (summed force and weighted average angles) are also shown. Sum temporalis vector (broken line) for *D. madagascariensis* not to scale.

represent genus *Varecia* with *V. rubra* as opposed to the *V. variegata* analyzed here, these taxa produce fertile offspring and are functionally color morphs that only recently have been elevated to separate species based primarily on conservation concerns. More importantly, they share virtually all ecomorphological characteristics and are thus considered equivalent herein from a myological perspective). Across 56 jaw adductor muscles (seven muscles each from eight taxa; literature data were unavailable for the corresponding jaw abductors), just 15 instances were observed in which fascicle lengths from the literature measured through traditional gross and chemical dissection fell outside even one standard deviation of our measured mean (Figure 7) and of these, only five comparisons (deep masseter and zygomatic temporalis in *Otolemur garnettii*; medial pterygoid in *D. madagascariensis*; zygomaticomandibularis in *E. mongoz*; and superficial masseter in *H. griseus*) fell outside of two standard deviations (i.e., a 95% confidence interval). While it should be noted that the fascicles measured by Perry et al. (2011, 2014) were collected from a combination of fixed and unfixed tissues, this difference in preservation is thought to be more impervious to fixation effects than muscle mass (as fascicle lengths are more strongly governed by the distance spanned between bony attachments, a spatial relationship that should not be altered by the effects of fixation; Leonard et al., 2022). Moreover, every effort was made to minimize the effects of preservation on muscle volumes (see above).

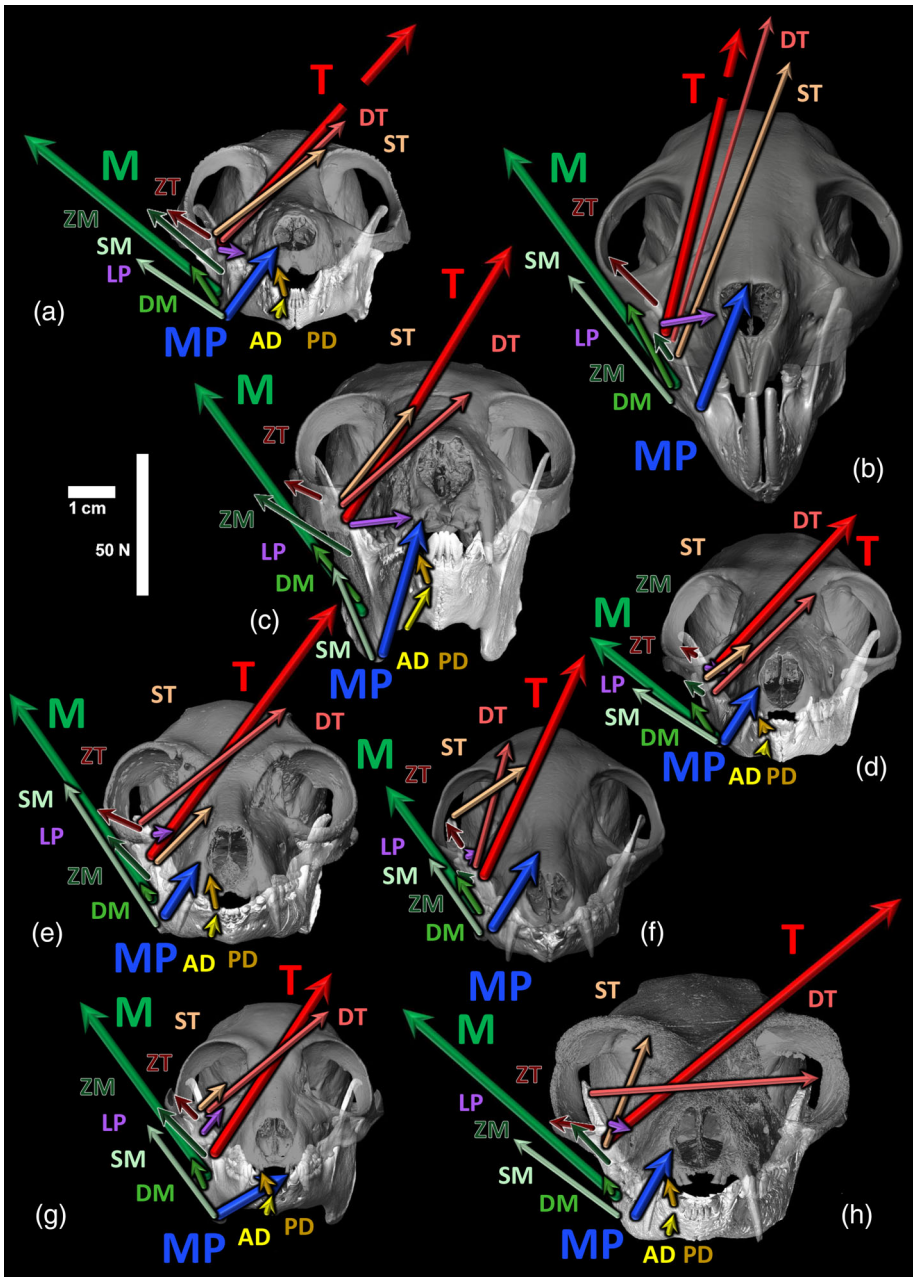

FIGURE 6 Anterior view of muscle vectors, depicting both paracoronal orientation and magnitude (see scale bars). Specimen identification and muscle vector coloration follow Figure 3; in addition, vectors of the masseter complex (M) and temporalis complex (T) (summed force and weighted average angles) are also shown. Sum temporalis vector (broken lines) for *O. garnettii* and *D. madagascariensis* not to scale.

Dietary effects on muscle architectural properties also followed previously reported trends. Relatively long adductor fascicles (i.e., strong positive residuals of fascicle length relative to body mass) were observed in the tree-gouging *D. madagascariensis* and frugivorous *Eulemur*, while relatively short fascicles (i.e., strong negative residuals) were observed in the folivorous *P. coquereli* (Figure 8). In terms of PCSA, the frugivorous/insectivorous *O. garnettii*, tree-gouging *D. madagascariensis*, and bamboo-specialist *H. griseus* all exhibited positive adductor residuals, while the strongest negative adductor residuals were observed in the frugivorous *V. variegata* and folivorous *P. coquereli* (Figure 8). Thus, prediction 1 was generally supported.

3.2 | Fascicle orientation

High degrees of variation in fascicle orientation (Table 1; Figures 2–4) were observed both within individual muscles and between muscle layers within a single group (e.g., between components of the masseteric complex). Layers of the masseter followed a consistent trend across all eight species wherein the most anteroposteriorly aligned fascicles were observed in the superficial masseter (ranging in parasagittal orientation from 18° in *V. variegata* to 54° in *P. coquereli*; average = 34°; Table 1; Figure 5). Deep masseter fascicles presented an intermediate orientation (ranging from 40° to 70°; average = 51.8°), while fascicles in the zygomaticomandibularis were close

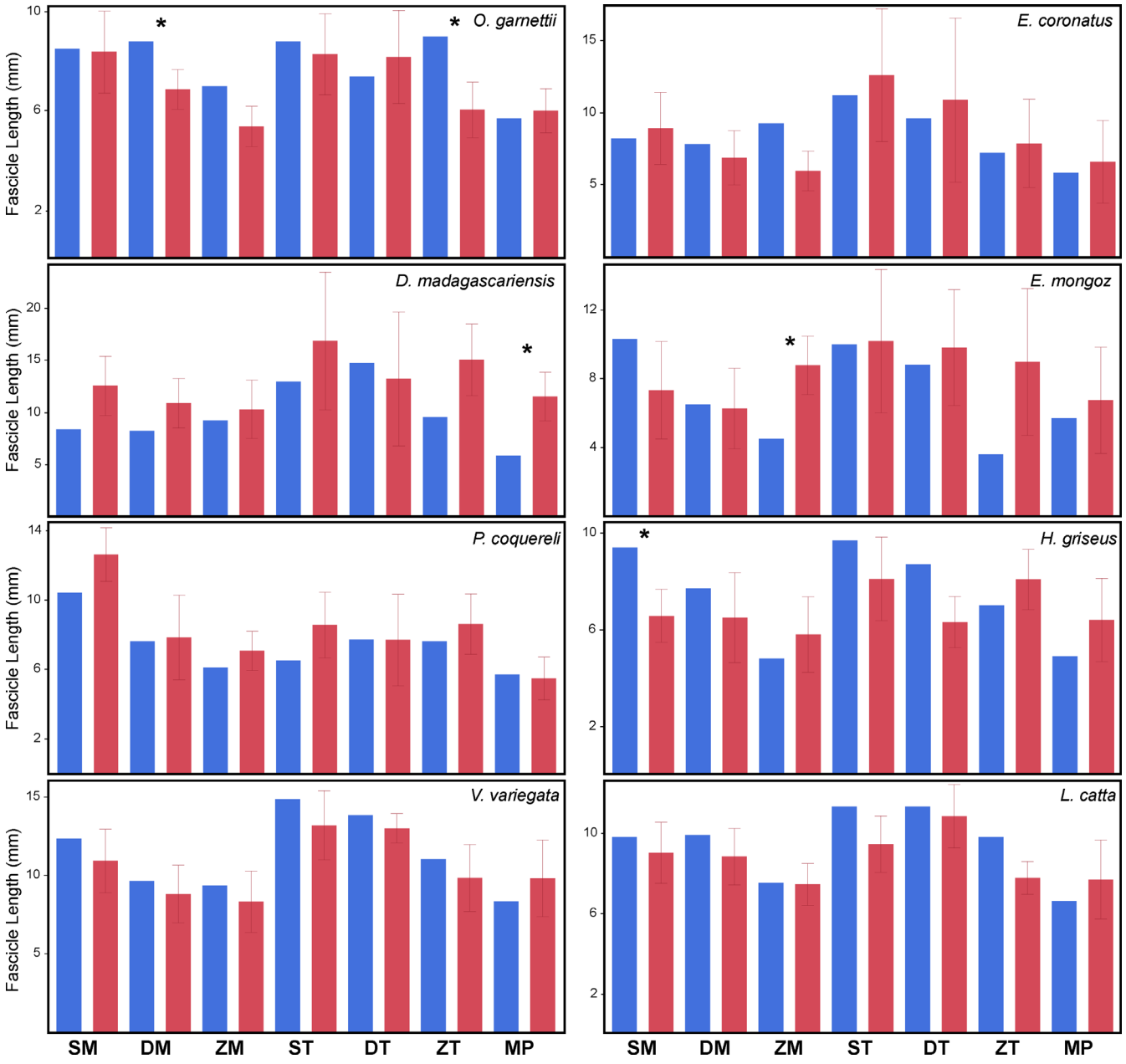

FIGURE 7 Comparison of fascicle lengths measured in this study (red) against literature-derived values of the equivalent muscles in conspecific individuals (blue). Error bars denote one standard deviation; asterisks denote that the literature value fell outside two standard deviations (i.e., 95%) of data from this study. Muscle abbreviations as follows: superficial masseter (SM), deep masseter (DM), zygomaticomandibularis (ZM), superficial temporalis (ST), deep temporalis (DT), zygomatic temporalis (ZT), and medial pterygoid (MP).

to vertical in orientation (81°-139°; average = 113°). By comparison, parasagittal orientations of the superficial and deep temporalis were generally similar (superficial temporalis = 134–161°, average = 147 ± 11°; deep temporalis = 139–157°, average = 149 ± 6°; Table 1 and Figure 5). Fascicles from the zygomatic temporalis were oriented slightly more anteroposteriorly (84–177°; average = 141 ± 32°). In most taxa, fascicles from the medial pterygoid shared similar parasagittal orientations to those of the deep masseter (medial pterygoid = 29–75°, average = 49 ± 16°; deep masseter = 40–69°, average = 55 ± 10°). Compared to the jaw adductor musculature, parasagittal orientations of the jaw abductors (lateral pterygoid, anterior digastric, and posterior digastric) were highly conservative between taxa. The former two ran anteroposteriorly in all cases (with the possible exception of *H. griseus* wherein fascicles from the LP were slightly more oblique) and, while fascicles from the posterior digastric were much more obliquely oriented, forces generated by the posterior digastric are ultimately translated into the anteroposterior

plane via the tendinous connection to the anterior digastric anchored on the hyoid (Dickinson et al., 2021; Gorniak, 1985).

Paracoronal fascicle orientations were generally tightly distributed between taxa (Figure 6). Layers of the masseter were relatively consistent both interspecifically and between muscles (superficial masseter = 23–56°, average = 40 ± 11°; deep masseter = 21–41°, average = 30 ± 6°; zygomaticomandibularis = 35–63°, average = 49 ± 8°; Figure 6). Fascicles from the zygomatic temporalis presented a similar orientation but with greater heterogeneity (33–84°, average = 56 ± 15°), while superficial temporalis and deep temporalis plotted more similarly to one another (ST = 305–341°, average = 322 ± 13°; DT = 274–345°, average = 315 ± 22°; Figure 6). Finally, as seen in the parasagittal plane, fascicles from the anterior and posterior digastric were highly consistent in orientation between species (anterior digastric = 14–32°, average = 20 ± 6°; posterior digastric = 329–347°, average = 340 ± 7°). Dietary associations with fascicle orientation were highly variable. In the superficial masseter, parasagittal fascicle orientationappeared to differentiate folivorous (wherein these fascicles were vertically oriented) from frugivorous taxa (wherein the fascicles were oblique or more anteroposterior in orientation). Additionally, highly folivorous taxa expressed masseter and temporalis parasagittal muscle vectors that intersected acutely, whereas frugivorous species (especially *V. variegata*) demonstrated masseter and temporalis vectors that intersect obliquely (Figure 5). Finally, in the paracoronal plane, folivorous species demonstrated a vertically oriented masseter, while this orientation was more obliquely mediolateral in frugivores. Thus, prediction 2 was partially supported.

3.3 | Fascicle tortuosity

Tortuosity was consistently greater within the jaw adductor muscles than within abductors but was similar in magnitude between the temporalis and masseter complex (Figure 9). Greater variation was observed between components of the temporalis complex than in the masseter. From an interspecific perspective, the greatest values were observed in the tree-gouging *D. madagascariensis* and the frugivores *V. variegata* and *E. mongoz*. Meanwhile, the lowest degree of tortuosity was seen in the bamboo specialist *H. griseus* (Figure 9). Thus, prediction 3 was generally supported.

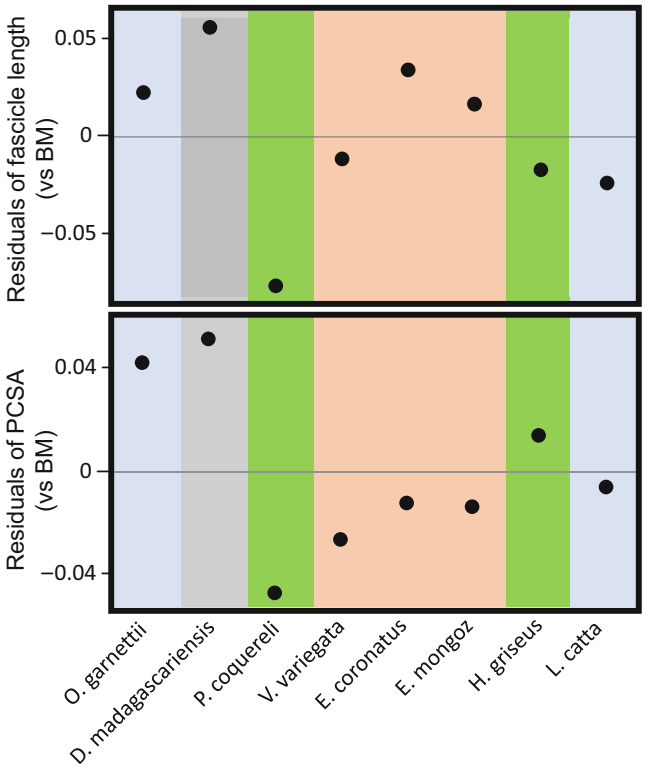

FIGURE 8 Plotted residuals of weighted-average jaw adductor fascicle lengths (top) and physiological cross-sectional area (PCSA; below) following reduced major axis regression against body mass. All variables were linearized and log-transformed prior to analysis. Background colors reflect the primary dietary category as follows: omnivory (blue), gouging (gray), folivory (green), and frugivory (orange); see Table 2 for full dietary information for each taxon.

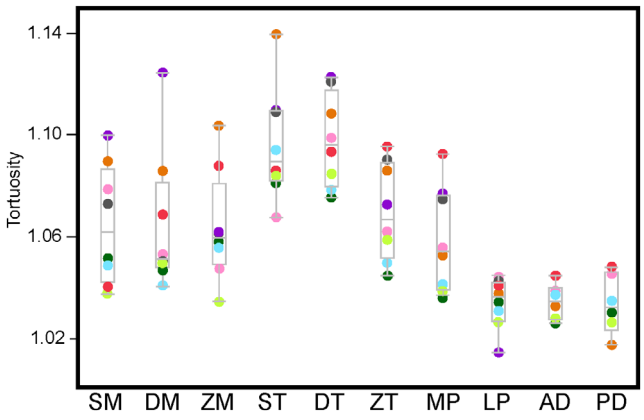

FIGURE 9 Tortuosity of fascicles within each muscle. As a metric of curved length to arc length, a tortuosity of 1 indicates linearity, and greater values indicate increased curvature. Muscle abbreviations as follows: superficial masseter (SM), deep masseter (DM), zygomaticomandibularis (ZM), superficial temporalis (ST), deep temporalis (DT), zygomatic temporalis (ZT), medial pterygoid (MP); lateral pterygoid (LP), anterior digastric (AD), posterior digastric (PD). Colored by species as follows: *Otolemur garnettii* (pink), *Daubentonia madagascariensis* (gray), *Propithecus coquereli* (dark green), *Varecia variegata* (orange), *Eulemur coronatus* (red), *Eulemur mongoz* (purple), *Hapalemur griseus* (light green), *Lemur catta* (blue).

4 | DISCUSSION

4.1 | Reconstructing fascicle lengths via DiceCT

Digital approaches to quantifying muscle architecture offer myriad potential benefits over traditional gross-dissection methods, including the circumvention of specimen destruction, enhanced specimen-sharing potential, and the preservation of three-dimensional spatial data. Accordingly, it is critical to understand the extent to which measurements collected using such techniques are comparable to those collected via gross dissection. To assess this, we compared fascicle lengths from our sample to previously published reports by Perry et al. (2011) and Perry et al. (2014). While some mismatches between data are expected (given the general intraspecific variation in this anatomy and that dissections were conducted on conspecific individuals of potentially different body sizes), we observed that fascicle lengths are mostly comparable between techniques (Figure 7). However, some directional bias was observed, with our digitally reconstructed fascicles typically shorter than those measured by Perry et al. (2011, 2014). The consistency of this difference would suggest some methodological impact, the most likely of which being a segmentation error in which fascicles were not traced to their final slice but instead ended preemptively. Alternatively, the gross/chemical dissection process may somehow relax the fascicles; however, we consider it to be more likely that the staining process may result in acidification-based muscle shrinkage (Dawood et al., 2021) that artificially reduces muscle volume and potentially alters architectural properties therein. While attempts were made to reduce such effects (including the use of both a sucrose prewash and low concentrations of I_2KI following Vickerton et al., 2013 and Gignac et al., 2016), this possibility cannot be discounted. Future studies should explicitly analyze such effects using a more tightly controlled sample (e.g., gross/chemical dissection vs. digital reconstruction of fascicles within the contralateral muscles of single individuals, while varying staining parameters across the sample). Likewise, as quantified in Leonard et al. (2022), it should be noted that formalin fixation of specimens prior to iodine staining may serve to slightly reduce muscle volumes, due to shrinkage—potentially lowering estimates of physiological cross-sectional area (PCSA). However, these effects are not considered sufficient to alter functional interpretations of masticatory adaptations within these taxa (Leonard et al., 2022).

While the number of fascicles measured herein is comparable to those collected via gross dissection, they are lower than recent studies that have employed algorithmic approaches to reconstructing fascicle lengths. As noted by Charles et al. (2022), the use of lower fascicle counts to represent a muscle increases the likelihood of inaccurate measurement profiles—a point strongly in favor of algorithmic processes. Certainly, as shown by Charles et al. (Figure 6b therein), increasing fascicle count reduces the standard deviation about the mean and, assuming similar accuracy of methods, increasing precision would also be desirable. However, as our own work on algorithmic reconstructions has previously shown (e.g., see Dickinson et al., 2018; Dickinson et al., 2023; Ratkiewicz et al., 2023), algorithmically reconstructed fascicles tend to yield greater errors on a per-fascicle basis than their manually segmented counterparts. Indeed, in many instances, these results can yield larger numbers of fascicles than are conceivably contained within a muscle—an artifact stemming either from double-counting of individual structures or from falsely identifying non-fascicular structures as valid objects of interest. However, recent work on standardizing protocols (see particularly Ratkiewicz et al., 2023) has begun to address this gulf, and it is hoped that in the coming years, validated algorithmic techniques that allow for the rapid assessment of >100 fascicles per muscle become standardized within the field.

4.2 | Dietary impacts on muscle architectural properties

As anticipated based on previously described relationships between fascicle lengths and food size—both in strepsirrhines (Perry et al., 2011) and other mammalian lineages (Hartstone-Rose et al., 2012; Hartstone-Rose et al., 2019; Hartstone-Rose et al., 2022)—frugivorous taxa (e.g., *E. coronatus*, *E. mongoz*, and *V. variegata*) and the wood-gouging *D. madagascariensis* all exhibited long jaw adductor fascicles for their respective body sizes. Meanwhile, the folivorous *P. coquereli* exhibited the shortest relative jaw adductor fascicles (Figure 8, top). One unanticipated finding, however, was the relatively high fascicle lengths observed in *O. garnettii*. Described as a mixed insectivore-frugivore (consuming approximately 50% of its diet from each category), *O. garnettii* was anticipated to exhibit relatively average fascicle lengths, similar to that of the generalist *L. catta*. Instead, *O. garnettii* exhibited the third-greatest relative fascicle lengths, exceeding those of both *E. mongoz* and *V. variegata*, the most frugivorous taxa in our sample.

We further observed that *O. garnettii* displayed the second-greatest relative PCSA values among our sample (Figure 8, bottom). Other taxa expressing positive residuals practice mechanically challenging diets (e.g., bamboo consumption in *H. griseus* and wood-gouging in *D. madagascariensis*) that

would theoretically require an elevated bite force potential, yet the diet of *O. garnettii* does not appear to exert similar demands. Though not directly discussed in the original manuscript, reanalysis of data presented by (Perry et al., 2011) across a larger subset of strepsirrhine taxa yielded the same finding: with *O. garnettii* exhibiting the highest relative bite force potential of any species (Perry et al., 2011). This taxon was also reported by Perry et al. (2011) as among the species with the longest relative jaw adductor fascicles, as seen in our own data. As this earlier study included numerous species of smaller body sizes than *O. garnettii*, the high positive residuals seen within our data cannot be ascribed to *O. garnettii* representing the smallest taxon within our sample. Instead, this would appear to represent a species signal that future studies of feeding behaviors in strepsirrhines may wish to explore in greater detail.

Furthermore, it is surprising to note that despite their theoretically demanding diets (Richard, 1977), *P. coquereli* exhibited a relatively low jaw adductor PCSA (Figure 8). *Propithecus coquereli* also demonstrated negative residuals in data presented by (Perry et al., 2011), albeit to a lesser degree. The relative reduction in bite force potential within *P. coquereli*, despite its mechanically challenging diet, may be of interest to future studies into strepsirrhine feeding performance.

4.3 | Interpreting variation in fascicle orientation

While substantial variation in fascicle orientations was observed between species, dietary associations are—in many cases—difficult to ascertain. For instance, the parasagittal orientation of fascicles in the superficial masseter follows a clear gradient of food toughness, being most vertically oriented in our two folivorous taxa (*P. coquereli* and *H. griseus*) and most anteroposteriorly oriented in our two most frugivorous species (*V. variegata* and *E. coronatus*). However, this pattern does not seem to extend to other layers of the masseteric complex.

Additionally, we observe that highly folivorous taxa (e.g., *H. griseus* and *P. coquereli*) express masseter and temporalis muscle vectors that intersect acutely, whereas frugivorous species (especially *V. variegata*) yield masseter and temporalis vectors that intersect obliquely (Figure 5). These trends appear to reflect a specific piece of bony anatomy, wherein folivores exhibit a taller mandibular ramus with a deeper masseteric fossa and a more vertically oriented area of attachment for the superficial masseter. We thus demonstrate that this anatomical configuration necessitates the reorganization of fascicles within the chewing musculature, altering the resultant vectors produced by muscle activation during mastication.

Furthermore, we note that in the paracoronal plane (Figure 6), folivorous species demonstrate a strongly vertical orientation of the masseter (36.2° and 36.3° in *H. griseus* and *P. coquereli*, respectively), while this orientation is more obliquely mediolateral in frugivores (e.g., 49.1° in *V. variegata*, 50.9° in *E. coronatus*). The same trend is observed in the temporalis, wherein folivores show a more vertical resultant vector (−33.2° and −30.8° in *H. griseus* and *P. coquereli*, respectively) than frugivores (−50.7° in *V. variegata* and −42° in *E. coronatus*). Again, this appears to reflect an underlying morphological factor: namely overall skull height relative to skull width, wherein folivores generally exhibit taller and relatively narrower skulls than frugivores (Figure 6). However, it must be noted that the current study utilizes only a single representative specimen per species. This makes it impossible to quantify degrees of intraspecific variation and also suggests that dietary interpretations made here should be evaluated further across larger sample sizes in future studies. This same shortcoming also applies to previous studies utilizing gross dissection (which also typically use only a single specimen per species), owing to the scarcity of well-preserved cadavers for rare primate species. Nevertheless, it is imperative that future studies endeavor to collect comparative data across larger samples to further verify the observations raised here. Similarly, it should be emphasized that skull morphology—itself constrained both by phylogeny and by other functional drivers beyond diet—is expected to contribute to and constrain potential variation in fascicle orientation.

4.4 | Fascicle tortuosity in a functional context

Fascicle tortuosity appeared to be relatively consistent between jaw adductor muscle groups, ranging from ∼103% to 110%. Little variation was observed between layers of the masseteric complex and the medial pterygoid, but tortuosity did appear to decline in the temporalis, being greatest in the superficial temporalis and lowest in the zygomatic temporalis (Figure 9). Tortuosity was generally greatest among frugivorous taxa (specifically *E. mongoz* and *V. variegata*) and in the tree-gouging *D. madagascariensis*, and lowest in the bamboo-specialist *H. griseus*. This may suggest a functional relationship between food item size and tortuosity, though trends were relatively variable (e.g., the unexpectedly high jaw adductor tortuosity seen in the folivorous *P. coquereli*). Additionally, we observed notably greater (2–3×) magnitudes of

fascicle tortuosity, as well as greater variation in tortuosity, within the jaw adductor musculature than in the jaw abductors. This trend is interpreted to reflect that sarcomeres within the jaw abductors sit close to their optimal resting length at jaw occlusion, a configuration which would optimize these muscles for gapes at or close to 0° in all analyzed taxa. By contrast, tortuosity in the jaw adductors may be more variable as a potential product of dietary differences (i.e., the sizes of either frequently consumed foods or the food size ranges at which adaptations to maximize adductive forces are necessary). While more explicit analyses across other taxonomic groups are necessary before any direct dietary inferences may be made, these data raise interesting and testable hypotheses to be assessed within future studies of three-dimensional fascicle organization.

5 | CONCLUSIONS

TheDiceCT toolkit has been used for several years as a relatively non-destructive means of assessing muscle architecture while preserving three-dimensional spatial information on fascicle configuration that would otherwise be unobservable. In this study—the largest interspecific sample of fascicular data yet analyzed using this methodology—we show that this method yields similar fascicle lengths and PCSA values as traditional gross dissection while also interpreting these new streams of data (e.g., fascicle orientation and tortuosity) within a functional context. We show that, among strepsirrhines, folivores and frugivores have different fascicle vector orientations and tortuosity—observations that enrich our understanding of adaptation in the primate masticatory apparatus. Importantly, as CT availability increases and new algorithmic approaches to digital dissection begin to yield comparable results to manual segmentation approaches, such data stand to be collected across even broader datasets in the coming years.

ACKNOWLEDGMENTS

We are grateful to editor Tim Smith, two anonymous reviewers and the organizations that provided the specimens used within this study and their staffs, and to Abigail Malach and Victoria Ledbetter for assistance with segmentation. We are also grateful to the Center for Biomedical Innovation at the New York Institute of Technology for providing computer software. This work was performed in part at the Duke University Shared Materials Instrumentation Facility (SMIF), a member of the North Carolina Research Triangle Nanotechnology Network (RTNN), which is supported by the National Science Foundation (award number ECCS-2025064) as part of the National Nanotechnology Coordinated Infrastructure (NNCI). This is Duke Lemur Center Publication 1574.

FUNDING INFORMATION

This project was funded in part by the National Sciences Foundation (IOS-5-57125) and by a New York Institute of Technology summer research grant to Aleksandra Ratkiewicz.

CONFLICT OF INTEREST STATEMENT

The authors have no competing interests to declare.

DATA AVAILABILITY STATEMENT

Raw data collected for this study are attached as supplementary data files.

ORCID

Edwin Dickinson https://orcid.org/0000-0002-9062-6677

Adam Hartstone-Rose https://orcid.org/0000-0001-5307-5573

REFERENCES

Anapol, F., & Barry, K. (1996). Fiber architecture of the extensors of the hindlimb in semiterrestrial and arboreal guenons. *American Journal of Physical Anthropology*, *99*(3), 429–447.

Anapol, F., Shahnoor, N., & Ross, C. F. (2008). Scaling of reduced physiologic cross-sectional area in primate muscles of mastication. In C. J. Vinyard, M. J. Ravosa, & C. E. Wall (Eds.), *Primate Craniofacial Function and Biology* (pp. 201–216). Springer US.

Antón, S. C. (1999). Macaque masseter muscle: Internal architecture, fiber length and cross-sectional area. *International Journal of Primatology*, *20*, 441–462.

Antón, S. C. (2000). Macaque pterygoid muscle: Internal architecture, fiber length, and cross-sectional area. *International Journal of Primatology*, *21*, 131–156.

Bang, M.-L., Li, X., Littlefield, R., Bremner, S., Thor, A., Knowlton, K. U., Lieber, R. L., & Chen, J. (2006). Nebulin-deficient mice exhibit shorter thin filament lengths and reduced contractile function in skeletal muscle. *The Journal of Cell Biology*, *173*(6), 905–916.

Baverstock, H., Jeffery, N. S., & Cobb, S. N. (2013). The morphology of the mouse masticatory musculature. *Journal of Anatomy*, *223*(1), 46–60.

Brand, R. A., Pedersen, D. R., & Friederich, J. A. (1986). The sensitivity of muscle force predictions to changes in physiologic cross-sectional area. *Journal of Biomechanics*, *19*(8), 589–596.

Britt, A. (2000). Diet and feeding behaviour of the black-and-white ruffed lemur (Varecia variegata variegata) in the Betampona Reserve, eastern Madagascar. *Folia Primatologica*, *71*(3), 133–141.

Campbell, J. L., Williams, C. V., & Eisemann, J. H. (2004). Use of total dietary fiber across four lemur species (Propithecus verreauxi coquereli, Hapalemur griseus griseus, Varecia variegata, and Eulemur fulvus): Does fiber type affect digestive efficiency? *American Journal of Primatology*, *64*(3), 323–335.

Carril, J., Degrange, F., & Tambussi, C. (2015). Jaw myology and bite force of the monk parakeet (Aves, Psittaciformes). *Journal of Anatomy*, *227*(1), 34–44.

Charles, J., Kissane, R., Hoehfurtner, T., & Bates, K. T. (2022). From fibre to function: Are we accurately representing muscle architecture and performance? *Biol Rev*, *97*, 1640–1676.

Chen, K. S., Li, J. Q., Rasoarahona, J., Folega, F., & Manjaribe, C. (2015). Diet and seed dispersal by *Eulemur coronatus* (Gray, primates and Lemuridae) in the Amber Mountain National Park, Madagascar. *International Journal of Biology*, *7*(4), 20.

Cox, P. G., & Faulkes, C. G. (2014). Digital dissection of the masticatory muscles of the naked mole-rat, *Heterocephalus glaber* (Mammalia, Rodentia). *PeerJ*, *2*, e448.

Cox, P. G., & Jeffery, N. (2011). Reviewing the morphology of the jaw-closing musculature in squirrels, rats, and Guinea pigs with contrast-enhanced microCT. *The Anatomical Record*, *294*(6), 915–928.

Curtis, D. J. (2004). Diet and nutrition in wild mongoose lemurs (Eulemur mongoz) and their implications for the evolution of female dominance and small group size in lemurs. *American Journal of Physical Anthropology*, *124*(3), 234–247.

Dawood, Y., Hagoort, J., Siadari, B., Ruijter, J., Gunst, Q., Lobe, N., Strijkers, G., de Bakker, B., & van den Hoff, M. (2021). Reducing soft-tissue shrinkage artefacts caused by staining with Lugol's solution. *Scientific Reports*, *11*(1), 1–12.

Deutsch, A. R., Dickinson, E., Leonard, K. C., Pastor, F., Muchlinski, M. N., & Hartstone-Rose, A. (2020). Scaling of anatomically derived maximal bite force in primates. *The Anatomical Record*, *303*(7), 2026–2035.

Dickinson, E., Atkinson, E., Meza, A., Kolli, S., Deutsch, A. R., Burrows, A. M., & Hartstone-Rose, A. (2020). Visualization and quantification of mimetic musculature via DiceCT. *PeerJ*, *8*, e9343.

Dickinson, E., Basham, C., Rana, A., & Hartstone-Rose, A. (2019). Visualization and quantification of digitally dissected muscle fascicles in the masticatory muscles of *Callithrix jacchus* using non-destructive DiceCT. *The Anatomical Record*, *302*, 1891–1900.

Dickinson, E., Fitton, L. C., & Kupczik, K. (2018). Ontogenetic changes to muscle architectural properties within the jaw-adductor musculature of Macaca fascicularis. *American Journal of Physical Anthropology*, *167*(2), 291–310.

Dickinson, E., Kolli, S., Schwenk, A., Davis, C. E., & Hartstone-Rose, A. (2020). DiceCT analysis of the extreme gouging adaptations within the masticatory apparatus of the aye-aye (*Daubentonia madagascariensis*). *The Anatomical Record*, *303*, 282–294.

Dickinson, E., Pastor, F., Santana, S. E., & Hartstone-Rose, A. (2021). Functional and ecological correlates of the primate jaw abductors. *The Anatomical Record*, *305*, 1245–1263.

Dickinson, E., Ratkiewicz, A., Granatosky, M. C., Molnar, J., & Hartstone-Rose, A. (2023). Algorithmic reconstruction of in situ muscle fascicles across a range of body sizes. Conference Proceedings; Society of Integrative and Comparative Biology Annual Meeting 2023 (Austin, TX).

Dickinson, E., Stark, H., & Kupczik, K. (2018). Non-destructive determination of muscle architectural variables through the use of DiceCT. *The Anatomical Record*, *301*, 363–377.

Early, C. M., Morhardt, A. C., Cleland, T. P., Milensky, C. M., Kavich, G. M., & James, H. F. (2020). Chemical effects of diceCT staining protocols on fluid-preserved avian specimens. *PLoS ONE*, *15*(9), e0238783.

Eng, C. M., Ward, S. R., Vinyard, C. J., & Taylor, A. B. (2009). The mechanics of the masticatory apparatus facilitate muscle force production at wide jaw gapes in tree-gouging marmosets (*Callithrix jacchus*). *Journal of Experimental Biology*, *212*, 4040–4055.

Erickson, C. J. (1991). Percussive foraging in the aye-aye, Daubentonia madagascariensis. *Animal Behaviour*, *41*(5), 793–801.

Erickson, C. J. (1994). Tap-scanning and extractive foraging in aye-ayes, *Daubentonia madagascariensis*. *Folia Primatologica*, *62*(1–3), 125–135.

Gans, C. (1982). Fiber architecture and muscle function. *Exercise and Sport Sciences Reviews*, *10*, 160–207.

Gans, C., & Bock, W. J. (1965). The functional significance of muscle architecture—a theoretical analysis. *Ergebnisse der Anatomie und Entwicklungsgeschichte*, *38*, 115–142.

Gignac, P. M., Kley, N. J., Clarke, J. A., Colbert, M. W., Morhardt, A. C., Cerio, D., Cost, I. N., Cox, P. G., Daza, J. D., Early, C. M., Echols, M. S., Henkelman, R. M., Herdina, A. N., Holliday, C. M., Li, Z., Mahlow, K., Merchant, S., Müller, J., Orsbon, C. P., ... Witmer, L. M. (2016). Diffusible iodine-based contrast-enhanced computed tomography (diceCT): An emerging tool for rapid, high-resolution, 3-D imaging of metazoan soft tissues. *Journal of Anatomy*, *228*(6), 889–909.

Gokhin, D. S., Bang, M.-L., Zhang, J., Chen, J., & Lieber, R. L. (2009). Reduced thin filament length in nebulin-knockout skeletal muscle alters isometric contractile properties. *American Journal of Physiology*, *296*(5), C1123–C1132.

Gorniak, G. C. (1985). Trends in the actions of mammalian masticatory muscles. *American Zoologist*, *25*, 331–337.

Grassi, C. (2006). Variability in habitat, diet, and social structure of Hapalemur griseus in Ranomafana National Park, Madagascar. *American Journal of Physical Anthropology*, *131*(1), 50–63.

Gussekloo, S. W., & Bout, R. G. (2005). Cranial kinesis in palaeognathous birds. *Journal of Experimental Biology*, *208*(17), 3409–3419.

Harcourt, C. S., & Nash, L. T. (1986). Species differences in substrate use and diet between sympatric galagos in two Kenyan coastal forests. *Primates*, *27*, 41–52.

Hartstone-Rose, A., Deutsch, A. R., Leischner, C. L., & Pastor, F. (2018). Dietary correlates of masticatory muscle fiber architecture in primates. *The Anatomical Record*, *301*, 311–324.

Hartstone-Rose, A., Dickinson, E., Deutsch, A. R., Worden, N., & Hirschkorn, G. A. (2022). Masticatory muscle architectural correlates of dietary diversity in Canidae, Ursidae, and across the order Carnivora. *The Anatomical Record*, *305*(2), 477–497.

Hartstone-Rose, A., Hertzig, I., & Dickinson, E. (2019). Bite force and masticatory muscle architecture adaptations in the dietarily diverse Musteloidea (Carnivora). *The Anatomical Record*, *302*(12), 2287–2299.

Hartstone-Rose, A., Perry, J. M., & Morrow, C. J. (2012). Bite force estimation and the fiber architecture of felid masticatory muscles. *The Anatomical Record*, *295*(8), 1336–1351.

Herrel, A., & O'Reilly, J. C. (2006). Ontogenetic scaling of bite force in lizards and turtles. *Physiological and Biochemical Zoology: PBZ*, *79*(1), 31–42.

Holliday, C. M., Sellers, K. C., Lessner, E. J., Middleton, K. M., Cranor, C., Verhulst, C. D., Lautenschlager, S., Bader, K., Brown, M. A., & Colbert, M. W. (2022). New frontiers in imaging, anatomy, and mechanics of crocodylian jaw muscles. *The Anatomical Record*, *305*, 3016–3030.

Holliday, C. M., Tsai, H. P., Skiljan, R. J., George, I. D., & Pathan, S. (2013). A 3D interactive model and atlas of the jaw musculature of Alligator mississippiensis. *PLoS ONE*, *8*(6), e62806.

Huyghe, K., Herrel, A., Adriaens, D., Tadić, Z., & Van Damme, R. (2009). It is all in the head: Morphological basis for differences in bite force among colour morphs of the Dalmatian wall lizard. *Biological Journal of the Linnean Society*, *96*(1), 13–22.

Jeffery, N. S., Stephenson, R. S., Gallagher, J. A., Jarvis, J. C., & Cox, P. G. (2011). Micro-computed tomography with iodine staining resolves the arrangement of muscle fibres. *Journal of Biomechanics*, *44*(1), 189–192.

Katzke, J., Puchenkov, P., Stark, H., & Economo, E. P. (2022). A roadmap to reconstructing muscle architecture from CT data. *Integrative Organismal Biology*, *4*(1), obac001.

Kay, R. F., Sussman, R. W., & Tattersall, I. (1978). Dietary and dental variations in the genus Lemur, with comments concerning dietary-dental correlations among Malagasy primates. *American Journal of Physical Anthropology*, *49*(1), 119–127.

Kikuchi, Y. (2010). Comparative analysis of muscle architecture in primate arm and forearm. *Anatomia, Histologia, Embryologia*, *39*(2), 93–106.

Kupczik, K., Stark, H., Mundry, R., Neininger, F. T., Heidlauf, T., & Röhrle, O. (2015). Reconstruction of muscle fascicle architecture from iodine-enhanced microCT images: a combined texture mapping and streamline approach. *Journal of Theoretical Biology*, *382*, 34–43.

Lanzetti, A., & Ekdale, E. G. (2021). Enhancing CT imaging: A safe protocol to stain and de-stain rare fetal museum specimens using diffusible iodine-based staining (diceCT). *Journal of Anatomy*, *239*(1), 228–241.

Leonard, K. C., Worden, N., Boettcher, M. L., Dickinson, E., & Hartstone-Rose, A. (2022). Effects of freezing and short-term fixation on muscle mass, volume, and density. *The Anatomical Record*, *305*(1), 199–208.

Li, Z., Clarke, J. A., Ketcham, R. A., Colbert, M. W., & Yan, F. (2015). An investigation of the efficacy and mechanism of contrast-enhanced X-ray computed tomography utilizing iodine for large specimens through experimental and simulation approaches. *BMC Physiology*, *15*(1), 5.

Lieber, R. L. (1986). Skeletal muscle adaptability. I: Review of basic properties. *Developmental Medicine & Child Neurology*, *28*(3), 390–397.

Lieber, R. L., & Fridén, J. (2000). Functional and clinical significance of skeletal muscle architecture. *Muscle & Nerve*, *23*(11), 1647–1666.

Marchi, D., Leischner, C. L., Pastor, F., & Hartstone-Rose, A. (2018). Leg muscle architecture in primates and its correlation with locomotion patterns. *The Anatomical Record*, *301*(3), 515–527.

Martinez, B. T., & Razafindratsima, O. H. (2014). Frugivory and seed dispersal patterns of the red-ruffed lemur, Varecia rubra, at a forest restoration site in Masoala National Park, Madagascar. *Folia Primatologica*, *85*(4), 228–243.

Metscher, B. D. (2009). MicroCT for comparative morphology: Simple staining methods allow high-contrast 3D imaging of diverse non-mineralized animal tissues. *BMC Physiology*, *9*(1), 11.

Mittermeier, R. A., Wilson, D. E., & Rylands, A. B. (2013). *Handbook of the mammals of the world: Primates*. Lynx Edicions.

Morhardt, A. C., & Witmer, L. M. (2016). *Diffusible iodine-based contrast enhancement of large, post-embryonic, intact vertebrates for CT scanning: Staining, destaining, and long-term storage*. ICVM.

Payne, R. C., Crompton, R. H., Isler, K., Savage, R., Vereecke, E. E., Günther, M. M., Thorpe, S., & D'Août, K. (2006). Morphological analysis of the hindlimb in apes and humans. I. Muscle Architecture. *Journal of Anatomy*, *208*(6), 709–724.

Penrose, F., Cox, P., Kemp, G., & Jeffery, N. (2020). Functional morphology of the jaw adductor muscles in the Canidae. *The Anatomical Record*, *303*, 2878–2903.

Perry, J. M., Hartstone-Rose, A., & Wall, C. E. (2011). The jaw adductors of strepsirrhines in relation to body size, diet, and ingested food size. *The Anatomical Record*, *294*(4), 712–728.

Perry, J. M., Macneill, K. E., Heckler, A. L., Rakotoarisoa, G., & Hartstone-Rose, A. (2014). Anatomy and adaptations of the chewing muscles in Daubentonia (Lemuriformes). *The Anatomical Record*, *297*(2), 308–316.

Pfaller, J. B., Gignac, P. M., & Erickson, G. M. (2011). Ontogenetic changes in jaw-muscle architecture facilitate durophagy in the turtle Sternotherus minor. *Journal of Experimental Biology*, *214*(10), 1655–1667.

Powell, P. L., Roy, R. R., Kanim, P., Bello, M. A., & Edgerton, V. R. (1984). Predictability of skeletal muscle tension from architectural determinations in Guinea pig hindlimbs. *Journal of Applied Physiology*, *57*(6), 1715–1721.

Ratkiewicz, A. S., Molnar, J., Khalil, A., Granatosky, M. C., & Dickinson, E. (2023). Multi-method analysis for the 3D quantification of muscle fascicle architecture. Conference Proceedings; Tomography for the Advancement of Science (ToScA), 2023 (Austin, TX).

Richard, A. (1977). The feeding behaviour of Propithecus verreauxi. In T. Clutton-Brock (Ed.), *Primate ecology: Studies of feeding and ranging behavior in lemurs, monkey and apes* (pp. 71–96). Elsevier.

Sahd, L., Bennett, N. C., & Kotzé, S. H. (2022). Hind foot drumming: Volumetric micro-computed tomography investigation of the hind limb musculature of three African mole-rat species (Bathyergidae). *Journal of Anatomy*, *240*(1), 23–33.

Sakamoto, M., Ruta, M., & Venditti, C. (2019). Extreme and rapid bursts of functional adaptations shape bite force in amniotes. *Proceedings of the Royal Society B*, *286*(1894), 20181932.

Santana, S. E. (2018). Comparative anatomy of bat jaw musculature via diffusible iodine-based contrast-enhanced computed tomography. *The Anatomical Record*, *301*, 267–278.

Sato, H., Santini, L., Patel, E. R., Campera, M., Yamashita, N., Colquhoun, I. C., & Donati, G. (2016). Dietary flexibility and feeding strategies of Eulemur: A comparison with Propithecus. *International Journal of Primatology*, *37*, 109–129.

Schumacher, G. (1961). *Funktionelle morphologie der kaumuskulatur*. Fisher.

Simmen, B., Hladik, A., & Ramasiarisoa, P. (2003). Food intake and dietary overlap in native Lemur catta and *Propithecus verreauxi* and introduced Eulemur fulvus at Berenty, Southern Madagascar. *International Journal of Primatology*, *24*, 949–968.

Simmen, B., Sauther, M. L., Soma, T., Rasamimanana, H., Sussman, R. W., Jolly, A., Tarnaud, L., & Hladik, A. (2006). Plant species fed on by Lemur catta in gallery forests of the southern domain of Madagascar. In A. Jolly, R. W. Sussman, N.

Koyama, & H. Rasamimanana (Eds.), *Ringtailed lemur biology* (pp. 55–68). Springer.

Sterling, E. J. (1994). Aye-ayes: Specialists on structurally defended resources. *Folia Primatologica*, *62*(1–3), 142–154.

Sullivan, S., McGechie, F., Middleton, K., & Holliday, C. (2019). 3D muscle architecture of the pectoral muscles of European Starling (*Sturnus vulgaris*). *Integrative Organismal Biology*, *1*(1), oby010.

Taylor, A. B., Eng, C. M., Anapol, F. C., & Vinyard, C. J. (2009). The functional correlates of jaw-muscle fiber architecture in tree-gouging and nongouging callitrichid monkeys. *American Journal of Physical Anthropology*, *139*(3), 353–367.

Taylor, A. B., & Vinyard, C. J. (2009). Jaw-muscle fiber architecture in tufted capuchins favors generating relatively large muscle forces without compromising jaw gape. *Journal of Human Evolution*, *57*(6), 710–720.

Taylor, A. B., & Vinyard, C. J. (2013). The relationships among jaw-muscle fiber architecture, jaw morphology, and feeding behavior in extant apes and modern humans. *American Journal of Physical Anthropology*, *151*(1), 120–134.

Terhune, C. E., Hylander, W. L., Vinyard, C. J., & Taylor, A. B. (2015). Jaw-muscle architecture and mandibular morphology influence relative maximum jaw gapes in the sexually dimorphic Macaca fascicularis. *Journal of Human Evolution*, *82*, 145–158.

To, K. H., O'Brien, H. D., Stocker, M. R., & Gignac, P. M. (2021). Cranial musculoskeletal description of black-throated finch (Aves: Passeriformes: Estrildidae) with DiceCT. *Integrative Organismal Biology*, *3*(1), obab007.

Toler, M. C., & Wall, C. E. (2013). Mandibular kinetics of gnawing in the aye-aye (*Daubentonia madagascariensis*) and biomechanical modeling of anterior tooth use. *American Journal of Physical Anthropology Abstract*, *150*, 272.

Turnbull, W. D. (1970). Mammalian masticatory apparatus. *Fieldiana: Geology*, *18*, 147–356.

Vickerton, P., Jarvis, J., & Jeffery, N. (2013). Concentration-dependent specimen shrinkage in iodine-enhanced micro CT. *Journal of Anatomy*, *223*(2), 185–193.

Weijs, W. A., & Hillen, B. (1985). Physiological cross-section of the human jaw muscles. *Cells Tissues Organs*, *121*(1), 31–35.

Yamashita, N., Vinyard, C. J., & Tan, C. L. (2009). Food mechanical properties in three sympatric species of Hapalemur in Ranomafana National Park, Madagascar. *American Journal of Physical Anthropology*, *139*(3), 368–381.

How to cite this article: Dickinson, E., Manzo, M., Davis, C. E., Kolli, S., Schwenk, A., Carter, A., Liu, C., Vasipalli, N., Ratkiewicz, A., Deutsch, A. R., Granatosky, M. C., & Hartstone-Rose, A. (2024). Ecological correlates of three-dimensional muscle architecture within the dietarily diverse Strepsirrhini. *The Anatomical Record*, *307*(6), 1975–1994. https://doi.org/10.1002/ar.25361